Mercury isotopes identify near-surface marine mercury in deep-sea trench biota

Joel D. Blum[a,1], Jeffrey C. Drazen[b], Marcus W. Johnson[a], Brian N. Popp[c], Laura C. Motta[a], and Alan J. Jamieson[d]

[a]Department of Earth and Environmental Sciences, University of Michigan, Ann Arbor, MI 48109; [b]Department of Oceanography, University of Hawaii at Manoa, Honolulu, HI 96822; [c]Department of Earth Sciences, University of Hawaii at Manoa, Honolulu, HI 96822; and [d]School of Natural and Environmental Sciences, Newcastle University, NE1 7RU Newcastle upon Tyne, United Kingdom

Mercury isotopic compositions of amphipods and snailfish from deep-sea trenches reveal information on the sources and transformations of mercury in the deep oceans. Evidence for methyl-mercury subjected to photochemical degradation in the photic zone is provided by odd-mass independent isotope values (Δ^{199}Hg) in amphipods from the Kermadec Trench, which average 1.57‰ ($\pm$0.14, n = 12, SD), and amphipods from the Mariana Trench, which average 1.49‰ ($\pm$0.28, n = 13). These values are close to the average value of 1.48‰ ($\pm$0.34, n = 10) for methyl-mercury in fish that feed at ~500-m depth in the central Pacific Ocean. Evidence for variable contributions of mercury from rainfall is provided by even-mass independent isotope values (Δ^{200}Hg) in amphipods that average 0.03‰ ($\pm$0.02, n = 12) for the Kermadec and 0.07‰ ($\pm$0.01, n = 13) for the Mariana Trench compared to the rainfall average of 0.13 ($\pm$0.05, n = 8) in the central Pacific. Mass-dependent isotope values (δ^{202}Hg) are elevated in amphipods from the Kermadec Trench (0.91 $\pm$0.22‰, n = 12) compared to the Mariana Trench (0.26 $\pm$0.23‰, n = 13), suggesting a higher level of microbial demethylation of the methyl-mercury pool before incorporation into the base of the foodweb. Our study suggests that mercury in the marine foodweb at ~500 m, which is predominantly anthropogenic, is transported to deep-sea trenches primarily in carrion, and then incorporated into hadal (6,000-11,000-m) food webs. Anthropogenic Hg added to the surface ocean is, therefore, expected to be rapidly transported to the deepest reaches of the oceans.

mercury | isotope | deep sea | trench | oceanography

Mercury (Hg) of both natural and anthropogenic origin circulates throughout the atmosphere and oceans. In the atmosphere gaseous elemental mercury [Hg(0)] has a residence time of about 1 y and is thus considered a global pollutant (1, 2). Deposition of mercury from the atmosphere to the land surface has been observed in even the most remote and pristine terrestrial ecosystems including the high Arctic tundra, Greenland, and Antarctica (3–6). This study investigates the sources and cycling of Hg in biota from deep-sea trenches, which are generally considered to be among the most remote and pristine ecosystems in the world's oceans (7, 8). Amphipods and snailfish were collected and analyzed for Hg isotopic composition and concentration from depths of 6,900–10,250 m in the Mariana Trench, ~320 km southwest of Guam in the northwest Pacific Ocean (12°N), and 6,000–10,000-m depths in the Kermadec Trench, ~400 km northeast of New Zealand in the southwest Pacific Ocean (32°S). For detailed locations see ref. 9. These trenches are among the deepest locations in the world's oceans.

Although much is known about the sources, concentrations, and transfer rates of Hg in the atmosphere, the inventories and dynamics of Hg in the oceans are much less well known. Recently, a few oceanographic studies have measured Hg biogeochemical parameters in biota and sinking particles in the relatively accessible upper ~1,000 m of the oceans (e.g., refs. 10–12). A general consensus has developed which suggests that Hg in the atmosphere can be deposited to the ocean surface as Hg(0) or photochemically

oxidized to form Hg(II), which is then deposited to the ocean surface primarily in rainfall. A portion of the deposited Hg(II) is microbially and abiotically reduced back to Hg(0) and returned to the atmosphere (13, 14). Hg(II) can also be microbially (11, 15) and abiotically (16–18) methylated in the water column. The oxygen minimum zone (OMZ, ~400–800 m in the central Pacific Ocean) appears to be the depth where methylating organisms occur and facilitate methylation (19). Some of the produced monomethyl-mercury (MMHg) may be advected to the photic zone, where it can be partially photochemically demethylated, and some may be demethylated microbially and abiotically below the OMZ (17, 18, 20).

Several studies have estimated what proportion of Hg in the oceans is anthropogenic, and into what water masses anthropogenic Hg has been transported (21, 22). Lamborg et al. (23) used the ratio of Hg to remineralized phosphorus in water masses to determine that about two-thirds of the anthropogenic Hg in the oceans was in the upper 1,000 m and that the Hg concentration in surface waters had approximately tripled compared to preindustrial times, suggesting that the Hg was ~70% anthropogenic. Outridge et al. (24) estimated that about 12% of the Hg transported to the deep ocean was of anthropogenic origin, but did not specifically consider transport to marine trenches. These conceptual models suggest that the proportion of anthropogenic Hg decreases with depth in the ocean and thus would be less

Significance

Mercury is a globally distributed neurotoxic pollutant that can be biomagnified in marine fish to levels that are harmful for consumption by humans and other animals. The degree to which mercury has infiltrated the oceans yields important information on the biogeochemistry of mercury and its expected effects on fisheries during changing mercury emissions scenarios. Mercury isotope measurement of biota from deep-sea trenches was used to demonstrate that surface-ocean-derived mercury has infiltrated the deepest locations in the oceans. It was found that when fish living in the surface ocean die and their carcasses sink (along with marine particles), they transfer large amounts of mercury to the trench foodwebs leading to high concentrations of mercury in trench biota.

Fig. 1. Depth of sample collection in meters on log scale versus δ^{202}Hg of samples. Symbol colors are keyed to the color of text labeling each sample type. Red and green symbols are analyses from this study of snailfish and amphipods from the Mariana (red) and Kermadec (green) trenches, respectively. Blue and black symbols are precipitation and marine particles from the central Pacific Ocean from ref. 12. Purple x's are analyses of fish from the central Pacific Ocean from refs. 26 and 12. See *SI Appendix*, Table S2 for analytical uncertainty of isotope values.

abundant in deep-sea trenches such as the Mariana and Kermadec trenches.

Much has been learned about the sources and cycling of Hg in the oceans from measurement of the stable isotopic compositions of Hg over the past decade (25–28). Hg has seven stable isotopes with nominal abundances of ^{196}Hg = 0.16%, ^{198}Hg = 10.0%, ^{199}Hg = 16.9%, ^{200}Hg = 23.1%, ^{201}Hg, =13.2%, ^{202}Hg = 29.7%, and ^{204}Hg = 6.83%; and their relative abundances can be measured with high precision in a wide range of sample types (29). During mass spectrometry analysis, each major isotope is referenced to ^{198}Hg, yielding five isotope ratios. Each isotope ratio for an environmental sample is referenced to a standard reference material (SRM-3133) and the deviation of the ratio from the standard is reported as a delta (δ) value in permil (‰). The δ^{202}Hg value is a measure of the difference in isotope ratios imparted by mass-dependent fractionation (MDF). Capital delta values (Δ) are a measure of the magnitude of mass-independent fractionation (MIF) for each isotope, that is, the difference in ‰ between the measured δ-value and the δ-value predicted for that isotope ratio due to MDF.

Based on isotope fractionation experiments and studies of Hg isotopes in environmental samples it has been found that there are six unique isotopic "signatures," each of which provides different clues to the complex biogeochemistry of Hg (30, 31). In some cases in this paper, we discuss the variation in "Δ" and "δ" values with depth in the ocean, which gives us a measure of the extent to which various reactions that affect Hg speciation have progressed and how this varies with depth. In other cases, we discuss the relationships between the various values of Δ and δ which yield information on the mechanisms of reactions that modify the chemical speciation of Hg in the oceans.

Results

Hg Concentrations. The Hg concentration (dry mass, see *SI Appendix*, Table S1) of snailfish muscle tissue from the Kermadec Trench ranges from 3.09 to 3.71 μg/g (average [ave.] 3.31 ± 0.35 μg/g, n = 3, SD) whereas the Mariana values range from 1.53 to 3.34 μg/g (ave. 2.38 ± 0.91 μg/g, n = 3). Amphipods display a much wider relative range of Hg concentrations with Kermadec amphipods ranging from 0.408 to 13.6 μg/g (ave. 3.54 ± 4.65 μg/g, n = 12) and Mariana amphipods ranging from 0.162 to 0.711 μg/g (ave. 0.338 ± 0.156 μg/g, n = 13). Note that the values following "±" throughout this paper represent SDs.

Hg Isotopic Composition. The Hg isotopic values fall into narrow ranges within each combined group of snailfish and amphipods analyzed at each site. In *SI Appendix*, Tables S1 and S2 we report the five delta values we use to fully describe changes in the isotopic composition of each sample. In all studies of Hg isotopes in biota Δ^{201}Hg has been shown to be strongly correlated with Δ^{199}Hg (in this study for all amphipods $r^2 = 0.98$; *SI Appendix*, Fig.S1). Similarly, Δ^{204}Hg has been shown to be correlated with Δ^{200}Hg, but with greater uncertainty because of the effects of analytical uncertainty for the relatively small Δ^{200}Hg and Δ^{204}Hg values (in this study for all amphipods $r^2 = 0.54$; *SI Appendix*, Fig. S2). For simplicity in our discussions below, we use Δ^{199}Hg values to describe the magnitude of odd MIF and Δ^{200}Hg values to describe the magnitude of even MIF.

δ^{202}Hg values of biota display a strong contrast between the two trenches (Fig. 1). For Kermadec snailfish, δ^{202}Hg values range from 1.02 to 1.05‰ (ave. 1.04 ± 0.02‰, n = 3) and Mariana values range from 0.43 to 0.65‰ (ave. 0.54 ± 0.16‰, n = 2). Kermadec δ^{202}Hg values for amphipods range from 0.56 to 1.39‰ (ave. 0.91 ±0.22‰, n = 12), whereas Mariana values for amphipods range from 0.02 to 0.70‰ (ave. 0.26 ± 0.23‰, n = 13). A Wilcoxon rank sum test (calculated using Microsoft Excel) for the amphipods yields a P value of <<0.01 indicating a significant difference in δ^{202}Hg values of amphipods between the two trenches.

Δ^{200}Hg values of biota also exhibit systematic differences between the two trenches (Fig. 2). Kermadec values for snailfish range from 0.018 to 0.022‰ (ave. 0.021 ± 0.003‰, n = 3) and Mariana values for snailfish range from 0.082 to 0.083‰ (ave. 0.083 ± 0.001‰, n = 2). Δ^{200}Hg values of amphipods in the Kermadec Trench (ave. 0.031 ± 0.020‰, range −0.010 to 0.060‰, n = 12) are lower than those in the Mariana Trench (ave. 0.069 ± 0.013‰, range 0.049 to 0.098‰, n = 13). A Wilcoxon rank sum test yields a P value of <<0.01 indicating a significant difference in Δ^{200}Hg values of amphipods between the two trenches.

In contrast to δ^{202}Hg and Δ^{200}Hg, Δ^{199}Hg values of biota in the two trenches are indistinguishable (Fig. 3). Kermadec Δ^{199}Hg values for snailfish range from 1.559 to 1.563‰ (ave.1.560 ± 0.002‰, n = 3). Values for Mariana snailfish range from 1.55 to 1.78‰ (ave.1.66 ± 0.16‰, n = 2). Kermadec Δ^{199}Hg values for amphipods average 1.57 ± 0.14‰ (range 1.38–1.79‰, n = 12), whereas Δ^{199}Hg values for Mariana amphipods average 1.49 ± 0.28‰ (range 1.13–2.31‰, n = 13). A Wilcoxon rank sum test yields a P value of 0.13, indicating that
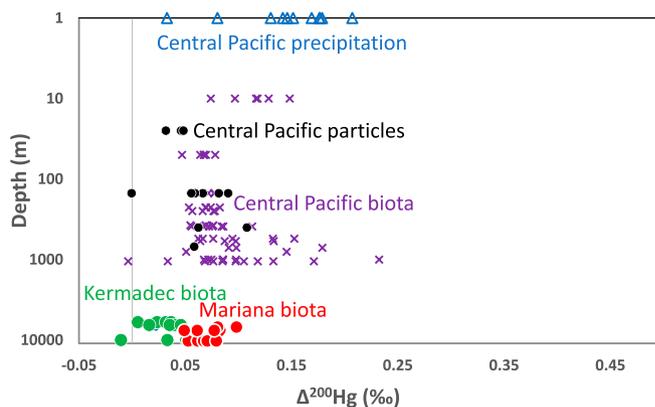
Fig. 2. Depth of sample collection in meters on log scale versus Δ^{200}Hg of samples. Symbols are the same as in Fig. 1. See *SI Appendix*, Table S2 for analytical uncertainty of isotope values.
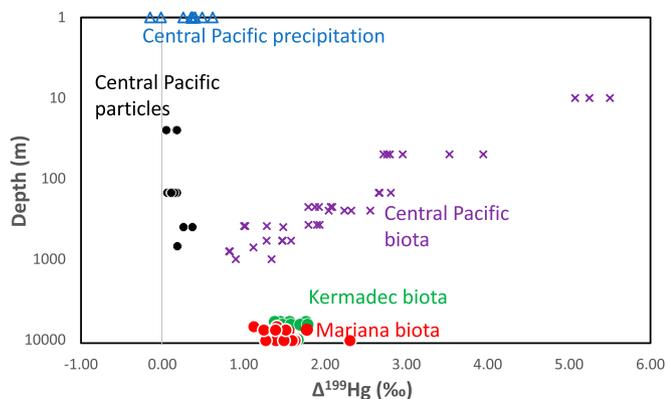
Fig. 3. Depth of sample collection in meters on log scale versus Δ^{199}Hg of samples. Symbols are the same as in Fig. 1. See *SI Appendix*, Table S2 for analytical uncertainty of isotope values.

the Δ^{199}Hg values of amphipods between the two trenches are not statistically different.

Discussion

Previous Work. Two papers that are closely related to our study were published recently. Liu et al. (32) measured Hg and monomethyl-Hg (MMHg) concentrations in amphipods collected from 6,990 to 10,840-m depth in the Massau, New Britain, and Mariana Trenches. They found that total-Hg (THg) and MMHg concentrations were higher in trench amphipods compared to amphipods from coastal and freshwater environments and suggested that this may be due to trench amphipods feeding on carrion from high trophic-level predators, which is consistent with fatty acid analyses of the same samples. Sun et al. (2020) measured THg and MMHg concentrations and Hg isotopic compositions of amphipods from the Mariana and nearby Yap Trench, as well as a single snailfish from the Yap Trench. They found that 2–59% of the Hg in amphipods (and 83% in the single snailfish) was in the form of MMHg, but they argued that the isotopic composition of THg in each sample was representative of the isotopic composition of MMHg in that sample because the inorganic Hg (IHg) in the biota was produced by in vivo degradation of MMHg rather than by assimilation of IHg. Sun et al. (33) provided four lines of evidence that make a strong case for the idea that IHg formed by degradation of MMHg. Our study and the study of Sun et al. (33) each measured THg and Hg isotopic composition of amphipods from the Mariana Trench. We have additionally measured Hg isotope ratios in amphipods from the Kermadec Trench and snailfish from both the Kermadec and Mariana trenches.

Odd MIF. Odd MIF in fish and other aquatic organisms is known to result exclusively from the photochemical degradation of MMHg dissolved in seawater and associated with dissolved organic carbon (DOC) (34). Remaining MMHg that is not degraded acquires elevated Δ^{199}Hg values, which scale with the proportion of MMHg that has been photodegraded (29). Blum et al. (26) and Motta et al. (12) analyzed the Hg isotopic composition of particles, fish, and zooplankton from the central Pacific Ocean and found that Δ^{199}Hg values were highest in flying fish feeding near the surface and declined in other biota with feeding depth down to 1,000 m. These authors suggested that MMHg was produced in the photic zone as well as deeper in the water column in the OMZ. Decreasing Δ^{199}Hg values with depth can only occur through addition of MMHg newly formed below the photic zone; consequently, this trend results from MMHg that has been near the

surface (and acquired high Δ^{199}Hg values) sinking through the water column on particles and the production of additional MMHg (with Δ^{199}Hg ~0‰) at greater depths, which is then added to these sinking particles lowering the foodweb Δ^{199}Hg values. It may also be possible that the MMHg is produced in the OMZ and advected to the photic zone where it is partially photochemically degraded before being transported back to greater depths. Given these conceptual models for variation in Δ^{199}Hg values with depth, one might expect organisms living at great depths in deep-sea trenches to have low Δ^{199}Hg values that approach zero.

Surprisingly, for the biota we measured from the Kermadec and Mariana trenches, Δ^{199}Hg values at 6,000–10,250 m are equivalent to values for biota at ~500-m depth (375–625 m) in the central Pacific Ocean (Fig. 3). Hadal zone (6,000–11,000-m) amphipods are opportunistic scavengers (e.g., ref. 35) and they rely on many types of organic matter for nutrition, including detritus and infauna as well as carrion falls (32, 36). Light stable isotope studies of hadal amphipods indicate wider ranges of δ^{15}N and δ^{13}C values compared to abyssal plain (3,000–6,000-m) species, suggesting extreme trophic diversity (36) and wide ranges of source amino acid- δ^{15}N values, which reflect a diversity in basal foodweb nutritional sources (9). Genetic analysis of amphipod stomach contents further confirms consumption of diatoms (from sinking particles), infauna, and pelagic carrion such as salps and tuna (36). Thus, amphipod diets likely integrate a variety of components and their Δ^{199}Hg values are likely indicative of the range of mercury sources to the hadal foodweb.

Total Hg in different size fractions of sinking particles (1–53 μm and >53 μm) in the central Pacific has Δ^{199}Hg values (12) that are much lower than in trench biota (Fig. 3). For particles to be the source of Hg to trench biota there would need to be a very small fraction of MMHg that has much higher Δ^{199}Hg values (~1.5‰), compared to the Δ^{199}Hg values for bulk particles from the central Pacific (ave. 0.16‰±0.09, $n = 12$; range 0.05–0.37‰). Bioaccumulation of a small, high-Δ^{199}Hg (1.5‰) MMHg fraction in particles could possibly provide the source of MMHg to trench biota. However, we find that a more parsimonious explanation is that an important component of the trench biota diet is carrion from fish that lived at a depth of ~500 m where the Δ^{199}Hg of fish averages about 1.5‰. We expect that the Δ^{199}Hg values of Hg reaching the trenches as carrion would be equivalent to a weighted average of Δ^{199}Hg values in fish sinking through the water column above the Kermadec and Mariana trenches. Recent studies have determined that mesopelagic (200–1,000-m depth) fish dominate the fish biomass of the oceans (37) and when mixed with fish from other depths could provide the appropriate Δ^{199}Hg value of the Hg flux to the trench environments.

The ratio of Δ^{199}Hg to Δ^{201}Hg values in fish and mammals from the world's oceans is remarkably constant at a value of ~1.2 (25, 27, 38–41). A York regression (42) of the hadal zone samples analyzed for this study yields a slope of 1.24 ± 0.02, whereas a York regression of fish from a range of depths in the mesopelagic of the central Pacific yield a slope of 1.23 ± 0.01. The consistency of Δ^{199}Hg/Δ^{201}Hg slopes suggests a common mechanism of photoreduction for the Hg bioaccumulated in the mesopelagic and the hadal zone biota. This is consistent with the generation of odd-MIF by photochemical degradation of MMHg in the photic zone and transfer of Hg from the mesopelagic to the hadal zones in sinking carrion.

Although sinking particles clearly transport some Hg to the deep ocean floor, low Δ^{199}Hg values of marine particles and zooplankton (ref. 12; Fig. 3), and low particulate MMHg concentrations (43, 44), suggest particles are probably not the dominant source of Hg to amphipods or snailfish in the Kermadec or Mariana trenches. Approximately 1% of the total Hg in sinking particles is in the form of MMHg (12, 43, 44) and the ratio of

MMHg to C is ~50× higher in mesopelagic fish (26) compared to particles in the central Pacific (~1,000 ng MMHg/g C versus ~20 ng MMHg/g C; Motta et al., ref. 12).

We argue that the flux of MMHg to the deep sea is most easily accounted for by carrion because they have the appropriate Δ^{199}Hg values and much higher ratios of MMHg/C. In addition, studies of the biogeochemical importance of carrion falls to the seafloor have concluded that a minimum of ~4% (45) and up to ~11% (46) of the organic carbon flux to the deep seafloor is from carrion. Since the MMHg/C ratio in average central Pacific fish compared to the ratio of MMHg to C in particles is about 50, if 4% of the organic carbon flux is from carrion, we calculate that at a minimum of 66% of the MMHg flux would be from carrion; if 11% of the organic carbon flux is from carrion, 86% of the MMHg flux would be from carrion.

Even MIF. Values for Δ^{200}Hg in biota are different for the two trenches, with statistically lower values for Kermadec (amphipods ave. 0.03‰±0.02, $n = 12$), and higher values for Mariana (amphipods ave. 0.07‰ ±0.01, $n = 13$) (Fig. 2). Even MIF is believed to be produced in the tropopause or stratosphere due to photochemical oxidation of Hg(0) by ultraviolet light (47, 48). Once produced and deposited to the Earth's surface the intensity of this isotopic signature can only be changed by mixing with another pool of Hg with contrasting Δ^{200}Hg. Rainfall in the central Pacific ranges in Δ^{200}Hg from 0.03 to 0.21‰ (ave. 0.13‰ ± 0.05, $n = 8$; ref. 12). Atmospheric Hg(0) on the Pacific Coast of North America (Mt. Bachelor, Oregon; ref. 49) ranges in Δ^{200}Hg from −0.05 to −0.17‰ (ave. −0.09‰ ± 0.04, $n = 26$). Biota in the central Pacific range in Δ^{200}Hg from 0.05 to 0.18‰ (ave. 0.08‰ ± 0.03, $n = 36$; refs. 12, 26).

One potential explanation for the higher even-MIF values in Mariana versus Kermadec biota is mixing of Hg from rainfall with either geogenic Hg from seafloor hydrothermal systems or turbidity flows, which would have Δ^{200}Hg values of ~0‰, or mixing with Hg(0) from the atmosphere, which would have Δ^{200}Hg values of ~ −0.09‰. A mix of about 50% geogenic Hg with rainfall-sourced Hg could shift the Mariana values to be equivalent to those of the Kermadec biota. A mix of about 25% atmospheric Hg(0) could also shift the Mariana values to be equivalent to those of the Kermadec biota. However, if this were a viable mechanism responsible for the difference in Δ^{200}Hg values between the two trenches, we would also expect input of geogenic or atmospheric Hg(0) to result in a lowering of Δ^{199}Hg values in Kermadec samples by about 50% due to mixing with either geogenic Hg or atmospheric Hg(0). Instead, we find that Δ^{199}Hg values of Kermadec biota are indistinguishable from Mariana Trench biota.

As an alternative explanation for the differing Δ^{200}Hg values of Kermadec versus Mariana biota, we suggest the possibility that the Δ^{200}Hg value of rainfall in the vicinity of the Kermadec Trench could be lower than in the vicinity of the Mariana Trench. There appears to be a latitudinal gradient by which Δ^{200}Hg values of northern hemisphere rainfall increases with latitude due to changes in mixing between the tropopause and the troposphere (48, 50). Although speculative and as yet unverified, we suggest the possibility that rainfall could have variable Δ^{200}Hg values in different global regions. We note that atmospheric modeling studies have demonstrated that atmospheric Hg in the southern hemisphere originates largely from the oceans rather than from the northern hemisphere atmosphere (14). In the northern hemisphere negative Δ^{204}Hg anomalies are preserved in precipitation in conjunction with positive Δ^{200}Hg anomalies, but with approximately twice the magnitude. When biota values for each trench are plotted as Δ^{200}Hg versus Δ^{204}Hg (*SI Appendix*, Fig. S1) we see that they display a slope of approximately −0.5, suggesting that the Hg

isotope trends observed in trench biota are formed by the same atmospheric oxidation fractionation mechanism that controls the even-MIF isotopic signature of rainfall.

MDF. In contrast to odd MIF, MDF values for hadal biota differ between the two trenches that we investigated. The Mariana Trench amphipods have lower δ^{202}Hg values (ave. 0.26 ± 0.23‰, $n = 13$), whereas the Kermadec Trench amphipods have higher δ^{202}Hg (ave. 0.91 ± 0.22‰, $n = 12$) (Fig. 3). It has been established experimentally that microbial degradation of MMHg results in an increase in the δ^{202}Hg value of remaining MMHg (51) that is then available for uptake into foodwebs. This is consistent with transport of MMHg via the tissues of carcasses to the trench floor where it is partially degraded by microbes with the remaining MMHg reincorporated into the foodweb. Methylation may also occur in this environment and this would lead to MDF in the opposite direction (lower δ^{202}Hg values in the MMHg). However, Cossa et al. (15) argued that demethylation dominated over methylation in the Mediterranean thermocline and we suggest that this may also be occurring in deep-ocean trench environments. Gerringer et al. (52) measured source amino acid δ^{15}N values in snailfish from the Kermadec and Mariana trenches and these values are higher in the Kermadec, consistent with greater bacterial reworking of particles at the base of the foodweb. Source amino acid values would propagate through the foodweb, so even if the main source of Hg to hadal organisms was carrion sinking from ~500 m, the Gerringer et al. (52) results on snailfish would still be consistent with this interpretation. Thus, microbial alteration is consistent with amino acid isotope data on amphipods and fish and is consistent with the trends we see in δ^{202}Hg values.

Combining MDF and Odd MIF. To summarize the various stages of Hg isotope fractionation that occur through the marine biogeochemical cycle, we include a plot of Δ^{199}Hg versus δ^{202}Hg with data from the central Pacific as well as the Kermadec and Mariana trenches. To help in the interpretation of trends in the data, we also include arrows indicating the trajectories for MDF and odd MIF based on experimental studies (Fig. 4). This graphic is meant to depict the minimum number of fractionation steps that we foresee occurring; the actual process could be more complex with Hg taking additional pathways. We begin with the addition of Hg(II) to the surface ocean in rainfall with an isotopic composition defined by measurements of rainfall collected
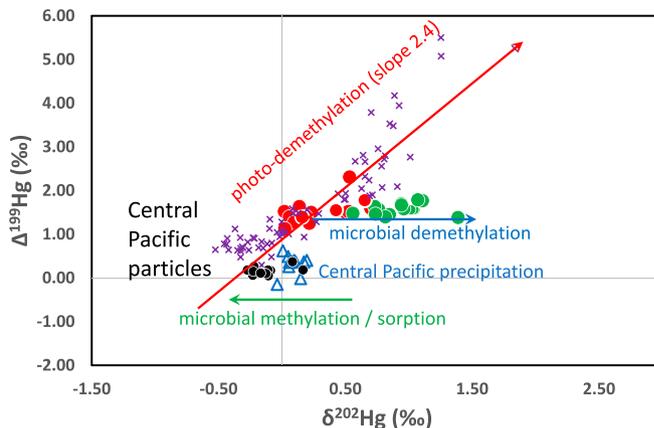
Fig. 4. Δ^{199}Hg versus δ^{202}Hg of all samples. Symbols are the same as in Fig. 1. Lines with arrows illustrate the shift in isotopic composition of residual MMHg during important fractionation processes (30). See *SI Appendix*, Table S2 for analytical uncertainty of isotope values.

shipboard and on the windward coast of the Island of Hawaii in the central Pacific (12). The first fractionation process, which shifts Hg(II) to lower δ^{202}Hg values, is consistent with particle sorption (12, 53, 54) or, alternatively, could be due to microbial methylation of a small fraction of the Hg(II) in ocean water (55, 56).

The second isotopic fractionation process is the photochemical reduction of MMHg attached to DOC and dissolved in water of the photic zone (0–100 m). As photodegradation proceeds both the Δ^{199}Hg and δ^{202}Hg values of the remaining MMHg (that eventually enters the foodweb) increase in magnitude with a slope of ~2.4 (29, 57). Flying fish have been used as a monitor of the maximum values of Δ^{199}Hg and δ^{202}Hg attained in the near-surface open ocean (58). As MMHg sinks through the photic zone and into the OMZ (~400–800 m in the central Pacific) it has been suggested that microbial production of MMHg occurs on particles (11) and in so doing dilutes the pool of MMHg with MMHg that is devoid of a positive Δ^{199}Hg value (26). As discussed above, the Δ^{199}Hg value of biota in the deep trenches is equivalent to values at ~500-m depth in the central Pacific. δ^{202}Hg values of Mariana biota are also the same as in the central Pacific at ~500-m depth, but δ^{202}Hg values in the Kermadec trench biota are higher by about 0.4–1.2‰. We suggest that these higher δ^{202}Hg values represent greater microbial degradation of MMHg during biogeochemical cycling in the water column and/or the hadal environment.

Conclusions

Hg isotope ratios of snailfish and amphipods from 6,000 to 10,250-m depth in the Mariana and Kermadec hadal trenches were measured and compared with Hg isotope measurements of a wide range of fish species in the central Pacific that feed at depths of 10–1,000 m. Based on odd-MIF and even-MIF isotopic signatures we conclude that the majority of Hg in the tissues of animals living in the hadal zone originates from the atmosphere, is methylated in the epipelagic (upper 200 m) and mesopelagic (200–1,000-m) zones, and is then delivered to the hadal zone (6,000–11,000 m) by the carcasses of fish, and to a lesser extent by particles (33). A near-surface source of Hg to hadal biota is consistent with recent documentation of "bomb ^{14}C" (59), lead (60), and persistent organic pollutants (61) in hadal biota. The importance of carrion to trench foodwebs is consistent with observations of seafloor communities of fish and amphipods that depend upon carrion for nutrition in other deep-sea regions (e.g., refs. 62–64). Sinking carcasses as a delivery mechanism provides a means for increasing the efficiency of the biological pump for Hg to the deep-seafloor in hadal environments and possibly also in abyssal settings.

Anthropogenic Hg enters the marine system via rainfall, dry deposition, and through runoff from rivers and estuaries. Some previous studies argued that the infiltration of this Hg into ocean water masses was mainly in the upper 1,000 m and that dissolved and particulate Hg in deep-ocean waters was largely preanthropogenic (e.g., ref. 23). Sun et al. (33) measured Hg isotopic compositions in amphipods from the Mariana Trench and concluded that Hg in them was transported from mesopelagic to hadal depths by sinking particles. With our present study, we find that the isotopic composition of Hg in sinking particles is inconsistent with that of trench biota and we suggest instead that the majority of Hg in trench biota was transported to the seafloor by carrion. Thus we provide evidence for a more direct vector that anthropogenic Hg can take from the surface ocean to the deep-ocean floor via the sinking of carcasses of animals. When scavengers such as snailfish and amphipods eat carrion, MMHg is transferred from the tissues of surface-dwelling organisms to tissues of bottom-dwelling organisms. Thus, we suggest that the majority of the Hg present in deep-sea trench organisms is derived from the mesopelagic ocean as indicated by identical Δ^{199}Hg values.

Materials and Methods

Sample Types and Sampling Procedures. Amphipods and snailfish were collected on the ocean floor in the Mariana (145E, 12N) and Kermadec (177W, 32S) deep-ocean trenches using full ocean depth lander vehicles equipped with baited traps [see Linley et al. (65) for details of sample locations and sampling techniques]. Twenty-five amphipods and six snailfish were analyzed from the two trenches: Kermadec (*Hirondellea dubia, Scopelocheirus schellenbergi,* and *Notoliparis kermadecensis*) and Mariana (*Alicella gigantea, Hirondellea gigas,* and *Pseudoliparis swirei*). Weight and length were measured upon recovery at the surface and samples were immediately frozen and kept frozen until they were freeze-dried in the laboratory. Work with fishes was approved by the University of Hawaii Institutional Animal Care and Use Committee program under protocol 11-1225 to J.C.D.

Analytical Methods. The Hg concentrations and isotopic compositions of biota were measured following methods identical to those used in previous studies of biota by the Michigan Mercury Isotope Laboratory (12, 25, 26). Details on specific procedures and reagent concentrations can be found in these previous publications. Briefly, freeze-dried whole specimens (amphipods) or muscle tissue (fish) were thermally decomposed in a two-stage tube furnace in a stream of O_2 and released Hg(0) was oxidized to Hg(II) and trapped in a solution of K-permanganate. An aliquot of this solution was measured for Hg concentration by atomic fluorescence spectrometry using an eight-point calibration curve and this yielded tissue total Hg concentrations. Hg(II) in the remaining K-permanganate solution was reduced to Hg(0) with SnCl and transferred in a stream of Hg-free air to another K-permanganate trap where it was oxidized to Hg(II). The yield of this purge and trap procedure was 98 ± 2%. Blanks prepared in the same manner as samples were determined to contribute an average of 0.12 ng Hg to sample Hg, or 0.3% ±0.2% (1 SD) of Hg processed per sample.

Hg isotopic composition was measured using a Nu-instruments multiple collector inductively coupled plasma mass spectrometer. Prior to isotope measurement sample solutions were adjusted to concentrations that ranged from 1 to 5 ng/g using Hg-free K-permanganate solution, which was also used to prepare concentration-matched bracketing-standard solutions of SRM-3133. Additional Hg-free permanganate solution was used for on-peak-zero measurements during mass-spectrometer sessions in order to monitor the effectiveness of signal washout between analyses. During isotope analysis a stream of gaseous Hg(0) was generated by online reduction of Hg(II) using $SnCl_2$ delivered with the sample to a frosted-tip phase separator, and combined with a Tl standard (SRM-997) added as a desolvated aerosol to the Hg(0) stream for mass-bias correction. Sample-standard bracketing was used for further mass-bias correction and for the determination of delta values for the Hg isotopes.

MDF is reported as δ^{202}Hg values in ‰ relative to SRM-3133 (Eq. **1**). MIF is the difference between the measured δ^{202}Hg value and that which would be predicted based on mass dependence using Eq. **2**, where *xxx* is the mass of each Hg isotope 199, 200, 201, 204, and β is the mass proportionality constant (0.2520, 0.5024, 0.7520, 1.493; ref. 66). Analytical results and uncertainties based on analyses of each isotope ratio in given in *SI Appendix*, Tables S1 and S2. SRMs used in this study included UM-Almaden, TORT-3, and DORM-4. The isotope values determined for preparations of these materials (*SI Appendix*, Table S2) are within uncertainty of published long-term average values for these materials (31). The larger 2 SD associated with each isotope value of either UM-Almaden or TORT-3 is assigned as the estimate of analytical uncertainty for each corresponding sample isotope value. Analytical results for all analyses of snailfish and amphipods from this study are given in *SI Appendix*, Table S1.

$$\delta Hg_{202} = \left(\left(\frac{\left(\frac{Hg_{202}}{Hg_{198}}\right)_{sample}}{\left(\frac{Hg_{202}}{Hg_{198}}\right)_{NIST3133}} \right) - 1 \right) \times 1{,}000, \qquad \text{[1]}$$

$$\Delta^{xxx}Hg \approx \delta^{xxx} - \left(\delta^{202} x \beta \right). \qquad \text{[2]}$$

Data Availability. All study data are included in the article and *SI Appendix*.

1. O. Lindqvist, H. Rodhe, Atmospheric mercury-a review. *Tellus* **37B**, 136–159 (1985).

2. C. T. Driscoll, R. P. Mason, H. M. Chan, D. J. Jacob, N. Pirrone, Mercury as a global pollutant: Sources, pathways, and effects. *Environ. Sci. Technol.* **47**, 4967–4983 (2013).

3. R. Ebinghaus *et al.*, Antarctic springtime depletion of atmospheric mercury. *Environ. Sci. Technol.* **36**, 1238–1244 (2002).

4. S. E. Lindberg *et al.*, Dynamic oxidation of gaseous mercury in the Arctic troposphere at polar sunrise. *Environ. Sci. Technol.* **36**, 1245–1256 (2002).

5. F. Sprovieri, N. Pirrone, I. M. Hedgecock, M. S. Landis, R. K. Stevens, Intensive atmospheric mercury measurements at Terra Nova Bay in Antarctica during november and december 2000. *J. Geophys. Res. Atmos.* **107**, 1–9 (2002).

6. W. Zheng, Z. Xie, B. A. Bergquist, Mercury stable isotopes in ornithogenic deposits as tracers of historical cycling of mercury in Ross sea, Antarctica. *Environ. Sci. Technol.* **49**, 7623–7632 (2015).

7. S. Dasgupta *et al.*, Toxic anthropogenic pollutants reach the deepest ocean on Earth. *Geochem. Perspect. Lett.* **7**, 22–26 (2018).

8. A. J. Jamieson *et al.*, Microplastics and synthetic particles ingested by deep-sea amphipods in six of the deepest marine ecosystems on Earth. *R. Soc. Open Sci.* **6**, 180667 (2019).

9. A. K. Tokuda *et al.*, Trophic interactions of megafauna in the Mariana and Kermadec trenches inferred from stable isotope analysis. *Deep Sea Res. Part I Oceanogr. Res. Pap.* **164**, 103360 (2020).

10. W. F. Fitzgerald, C. H. Lamborg, C. R. Hammerschmidt, Marine biogeochemical cycling of mercury. *Chem. Rev.* **107**, 641–662 (2007).

11. E. M. Sunderland, D. P. Krabbenhoft, J. W. Moreau, S. A. Strode, W. M. Landing, Mercury sources, distribution, and bioavailability in the North Pacific Ocean: Insights from data and models. *Global Biogeochem. Cycles* **23**, 1–14 (2009).

12. L. C. Motta *et al.*, Mercury cycling in the North Pacific Subtropical Gyre as revealed by mercury stable isotope ratios. *Global Biogeochem. Cycles* **33**, 777–794 (2019).

13. R. P. Mason *et al.*, The air-sea exchange of mercury in the low latitude Pacific and Atlantic Oceans. *Deep Sea Res. Part A* **122**, 17–28 (2017).

14. H. M. Horowitz *et al.*, A new mechanism for atmospheric mercury redox chemistry: Implications for the global mercury budget. *Atmos. Chem. Phys.* **17**, 6353–6371 (2017).

15. D. Cossa, B. Averty, N. Pirrone, The origin of methylmercury in open mediterranean waters. *Limnol. Oceanogr.* **54**, 837–844 (2009).

16. M. Monperrus *et al.*, Mercury methylation, demethylation and reduction rates in coastal and marine surface waters of the Mediterranean Sea. *Mar. Chem.* **107**, 49–63 (2007).

17. K. M. Munson, C. H. Lamborg, R. M. Boiteau, M. A. Saito, Dynamic mercury methylation and demethylation in oligotrophic marine water. *Biogeosciences* **15**, 6451–6460 (2018).

18. K. Wang, K. M. Munson, D. A. Armstrong, R. W. Macdonald, F. Wang, Determining seawater mercury methylation and demethylation rates by the seawater incubation approach: A critique. *Mar. Chem.* **219**, 103753 (2020).

19. E. Villar, L. Cabrol, L. E. Heimbürger-Boavida, Widespread microbial mercury methylation genes in the global ocean. *Environ. Microbiol. Rep.* **12**, 277–287 (2020).

20. R. P. Mason, G. Sheu, Role of the ocean in the global mercury cycle. *Global Biogeochem. Cycles* **16**, 1093 (2002).

21. E. M. Sunderland, R. P. Mason, Human impacts on open ocean mercury concentrations. *Global Biogeochem. Cycles* **21**, 2876 (2007).

22. D. G. Streets *et al.*, All-time releases of mercury to the atmosphere from human activities. *Environ. Sci. Technol.* **45**, 10485–10491 (2011).

23. C. H. Lamborg *et al.*, A global ocean inventory of anthropogenic mercury based on water column measurements. *Nature* **512**, 65–68 (2014).

24. P. M. Outridge, R. P. Mason, F. Wang, S. Guerrero, L. E. Heimbürger-Boavida, Updated global and oceanic mercury budgets for the United Nations global mercury assessment 2018. *Environ. Sci. Technol.* **52**, 11466–11477 (2018).

25. D. B. Senn *et al.*, Stable isotope (N, C, Hg) study of methylmercury sources and trophic transfer in the northern gulf of Mexico. *Environ. Sci. Technol.* **44**, 1630–1637 (2010).

26. J. D. Blum, B. N. Popp, J. C. Drazen, C. Anela Choy, M. W. Johnson, Methylmercury production below the mixed layer in the north Pacific Ocean. *Nat. Geosci.* **6**, 879–884 (2013).

27. D. J. Madigan *et al.*, Mercury stable isotopes reveal influence of foraging depth on mercury concentrations and growth in Pacific bluefin tuna. *Environ. Sci. Technol.* **52**, 6256–6264 (2018).

28. M. Štrok, P. A. Baya, H. Hintelmann, The mercury isotope composition of Arctic coastal seawater. *C. R. Geosci.* **347**, 368–376 (2015).

29. B. A. Bergquist, J. D. Blum, Mass-dependent and -independent fractionation of hg isotopes by photoreduction in aquatic systems. *Science* **318**, 417–420 (2007).

30. J. D. Blum, L. S. Sherman, M. W. Johnson, Mercury isotopes in Earth and environmental Sciences. *Annu. Rev. Earth Planet. Sci.* **42**, 249–269 (2014).

31. J. D. Blum, M. W. Johnson, Recent developments in mercury stable isotope analysis. *Rev. Mineral. Geochem.* **82**, 733–757 (2017).

32. M. Liu *et al.*, Methylmercury bioaccumulation in deepest ocean fauna: Implications for ocean mercury biotransport through food webs. *Environ. Sci. Technol. Lett.* **7**, 469–476 (2020).

33. R. Sun *et al.*, Methylmercury produced in upper oceans accumulates in deep Mariana Trench fauna. *Nat. Commun.* **11**, 3389 (2020).

34. B. P. DiMento, R. P. Mason, Factors controlling the photochemical degradation of methylmercury in coastal and oceanic waters. *Mar. Chem.* **196**, 116–125 (2017).

35. A. J. Jamieson *et al.*, Bait-attending fauna of the Kermadec trench, SW Pacific Ocean: Evidence for an ecotone across the abyssal-hadal transition zone. *Deep Sea Res. Part A* **58**, 49–62 (2011).

36. L. E. Blankenship, L. A. Levin, Extreme food webs: Foraging strategies and diets of scavenging amphipods from the ocean's deepest 5 kilometers. *Limnol. Oceanogr.* **52**, 1685–1697 (2007).

37. X. Irigoien *et al.*, Large mesopelagic fishes biomass and trophic efficiency in the open ocean. *Nat. Commun.* **5**, 3271 (2014).

38. M. Li *et al.*, Environmental origins of methylmercury accumulated in subarctic estuarine fish indicated by mercury stable isotopes. *Environ. Sci. Technol.* **50**, 11559–11568 (2016).

39. M. Li *et al.*, Selenium and stable mercury isotopes provide new insights into mercury toxicokinetics in pilot whales. *Sci. Total Environ.* **710**, 136325 (2020).

40. S. Y. Kwon, J. D. Blum, C. Y. Chen, D. E. Meattey, R. P. Mason, Mercury isotope study of sources and exposure pathways of methylmercury in estuarine food webs in the Northeastern U.S. *Environ. Sci. Technol.* **48**, 10089–10097 (2014).

41. D. K. Sackett *et al.*, Carbon, nitrogen, and mercury isotope evidence for the biogeochemical history of mercury in Hawaiian marine bottomfish. *Environ. Sci. Technol.* **51**, 13976–13984 (2017).

42. D. York, N. M. Evensen, M. López Martinez, J. D. B. Delgado, Unified equations for the slope, intercept, and standard errors of the best straight line. *Am. J. Phys.* **367**, 367–375 (2004).

43. C. R. Hammerschmidt, K. L. Bowman, Vertical methylmercury distribution in the subtropical North Pacific Ocean. *Mar. Chem.* **132–133**, 77–82 (2012).

44. K. M. Munson, C. H. Lamborg, G. J. Swarr, M. A. Saito, Mercury species concentrations and fluxes in the central tropical Pacific Ocean. *Global Biogeochem. Cycles* **29**, 656–676 (2015).

45. N. D. Higgs, A. R. Gates, D. O. B. Jones, Fish food in the deep sea: Revisiting the role of large food-falls. *PLoS One* **9**, e96016 (2014).

46. C. R. Smith, Food for the deep sea: Utilization, dispersal, and flux of Nekton Falls at the Santa Catalina basin floor. *Deep Sea Res. Part A* **32**, 417–442 (1985).

47. J. Chen, H. Hintelmann, X. Feng, B. Dimock, Unusual fractionation of both odd and even mercury isotopes in precipitation from Peterborough, ON, Canada. *Geochim. Cosmochim. Acta* **90**, 33–46 (2012).

48. Z. Wang *et al.*, Mass-dependent and mass-independent fractionation of mercury isotopes in precipitation from Guiyang, SW China. *C. R. Geosci.* **347**, 358–367 (2015).

49. A. Y. Kurz, J. D. Blum, L. E. Gratz, D. A. Jaffe, Anthropogenic impacts on the atmosphere contrasting controls on the diel isotopic variation of Hg0 at two high elevation sites in the Western United States. *Environ. Sci. Technol.* **54**, 10502–10513 (2020).

50. H. Cai, J. Chen, Mass-independent fractionation of even mercury isotopes. *Sci. Bull. (Beijing)* **61**, 116–124 (2016).

51. K. Kritee, T. Barkay, J. D. Blum, Mass dependent stable isotope fractionation of mercury during mer mediated microbial degradation of monomethylmercury. *Geochim. Cosmochim. Acta* **73**, 1285–1296 (2009).

52. M. E. Gerringer, B. N. Popp, T. D. Linley, A. J. Jamieson, J. C. Drazen, Comparative feeding ecology of abyssal and hadal fishes through stomach content and amino acid isotope analysis. *Deep Sea Res. Part A* **121**, 110–120 (2017).

53. M. Jiskra *et al.*, Kinetics of Hg(II) exchange between organic ligands, goethite, and natural organic matter studied with an enriched stable isotope approach. *Environ. Sci. Technol.* **48**, 13207–13217 (2014).

54. J. G. Wiederhold *et al.*, Equilibrium mercury isotope fractionation between dissolved Hg(II) species and thiol-bound Hg. *Environ. Sci. Technol.* **44**, 4191–4197 (2010).

55. P. Rodríguez-González *et al.*, Species-specific stable isotope fractionation of mercury during Hg(II) methylation by an anaerobic bacteria (Desulfobulbus propionicus) under dark conditions. *Environ. Sci. Technol.* **43**, 9183–9188 (2009).

56. S. E. Janssen, J. K. Schaefer, T. Barkay, J. R. Reinfelder, Fractionation of mercury stable isotopes during microbial methylmercury production by iron- and sulfate-Reducing bacteria. *Environ. Sci. Technol.* **50**, 8077–8083 (2016).

57. P. Chandan, S. Ghosh, B. A. Bergquist, Mercury isotope fractionation during aqueous photoreduction of monomethylmercury in the presence of dissolved organic matter. *Environ. Sci. Technol.* **49**, 259–267 (2015).

58. L. C. Motta, J. D. Blum, B. N. Popp, J. C. Drazen, H. Close, Mercury stable isotopes in flying fish as a monitor of photochemical degradation of methylmercury in the atlantic and Pacific oceans. *Mar. Chem.* **223**, 103790 (2020).

59. N. Wang et al., Penetration of bomb 14C into the deepest ocean trench. *Geophys. Res. Lett.* **46**, 5413–5419 (2019).

60. C. J. Welty, M. L. Sousa, F. M. Dunnivant, P. H. Yancey, High-density element concentrations in fish from subtidal to hadal zones of the Pacific Ocean. *Heliyon* **4**, e00840 (2018).

61. A. J. Jamieson, T. Malkocs, S. B. Piertney, T. Fujii, Z. Zhang, Bioaccumulation of persistent organic pollutants in the deepest ocean fauna. *Nat. Ecol. Evol.* **1**, 51 (2017).

62. J. C. Drazen et al., Bypassing the abyssal benthic food web: Macrourid diet in the eastern North Pacific inferred from stomach content and stable isotopes analyses. *Limnol. Oceanogr.* **53**, 2644–2654 (2008).

63. J. C. Drazen, R. L. Haedrich, A continuum of life histories in deep-sea demersal fishes. *Deep Sea Res. Part A* **61**, 34–42 (2012).

64. H. J. T. Hoving, S. L. Bush, S. H. D. Haddock, B. H. Robison, Bathyal feasting: Post-spawning squid as a source of carbon for deep-sea benthic communities. *Proc. Biol. Sci.* **284**, 10–12 (2017).

65. T. D. Linley et al., Fishes of the hadal zone including new species, in situ observations and depth records of Liparidae. *Deep Sea Res. Part A* **114**, 99–110 (2016).

66. J. D. Blum, B. A. Bergquist, Reporting of variations in the natural isotopic composition of mercury. *Anal. Bioanal. Chem.* **388**, 353–359 (2007).